Combinatorial Chemical Vapor Deposition. Achieving Compositional Spreads of Titanium, Tin, and Hafnium Oxides by Balancing Reactor Fluid Dynamics and Deposition Kinetics

Ryan C. Smith,[†] Noel Hoilien,[‡] Jimmy Chien,[‡] Stephen A. Campbell,[‡] Jeffrey T. Roberts,[†] and Wayne L. Gladfelter*,[†]

Department of Chemistry and Department of Electrical and Computer Engineering, University of Minnesota, Minneapolis, Minnesota 55455

Received September 6, 2002. Revised Manuscript Received October 29, 2002

A low-pressure chemical vapor deposition (CVD) reactor was modified to produce a continuous compositional spread of titanium, tin, and hafnium dioxides on a single Si(100) wafer. The corresponding anhydrous metal nitrates, $Ti(NO_3)_4$, $Sn(NO_3)_4$, and $Hf(NO_3)_4$, were used as single-source precursors to the component oxides. The compositions were mapped using X-ray photoelectron spectroscopy and Rutherford backscattering spectrometry. On a single wafer an array of 100 μm × 100 μm capacitors was used to map the effective dielectric constant (κ_{eff}) of the films. For compositional spreads grown at 400 and 450 °C κ_{eff} reached a maximum value in regions with the highest concentrations of TiO_2. The formation of the orthorhombic α-PbO_2 phase for a composition near $Hf_{0.75}Sn_{0.25}O_2$ was also observed in the 450 °C compositional spread.

Introduction

The need to develop an alternative material for the gate dielectric in field effect transistors has focused attention on many monometallic metal oxides (e.g., TiO_2, ZrO_2, HfO_2, Ta_2O_5, Al_2O_3, etc.) and several compound oxides, such as $SrTiO_3$. Other attractive candidates include silicon nitride and the mixed nitride/oxide of silicon.[1,2] Another approach has involved the co-deposition of a high κ material with a glass-forming oxide (e.g., SiO_2 or Al_2O_3) to produce an amorphous, low-leakage current film that still has an acceptably high value of κ.[3] Even for a two-component mixture, exploring all possible compositions requires many depositions. For films deposited by CVD using multiple precursors, optimization of the composition can be further complicated because the stoichiometry of the final film may not necessarily reflect the ratio of the precursor mixture.

There has been a resurgence of interest in developing high-throughput methods for identification of new materials. Van Dover et al. used an off-axis reactive sputtering method to produce a continuous compositional spread (CS) of three metal oxides that allowed the rapid determination of an optimum stoichiometry based on a combination of electrical measurements made on a single wafer.[4−6] For the $ZrO_2/SnO_2/TiO_2$ system, this stoichiometry corresponded to $Zr_{0.2}Sn_{0.2}Ti_{0.6}O_2$. Despite the close similarity between Zr and Hf, the same experiment established a different ratio for the $HfO_2/SnO_2/TiO_2$ system ($Hf_{0.2}Sn_{0.05}Ti_{0.75}O_2$).[7]

The use of CVD to produce compositional spreads in multicomponent systems has been limited, and, to the best of our knowledge, none exist for multicomponent oxides.[8,9] This paper describes the design of a CVD reactor that can produce compositional variation. To achieve precursor compatibility, gas-phase reactions must be minimized while maintaining approximately similar growth rates. This suggests precursors with similar deposition chemistry (i.e., similar ligands) may be good starting points. In this lab, the anhydrous metal nitrates $Hf(NO_3)_4$, $Sn(NO_3)_4$, and $Ti(NO_3)_4$ have been established previously as single source CVD precursors to the pure metal dioxide films.[10−14] Herein, we describe

* To whom correspondence should be addressed (phone 612-624-4391; fax 612-626-8659; e-mail gladfelt@chem.umn.edu).
[†] Department of Chemistry.
[‡] Department Electrical and Computer Engineering.

(1) Wilk, G. D.; Wallace, R. M.; Anthony, J. M. *J. Appl. Phys.* **2001**, *89*, 5243−5275.
(2) Buchanan, D. A. *IBM J. Res. Dev.* **1999**, *43*, 245−264.
(3) Wilk, G. D.; Wallace, R. M.; Anthony, J. M. *J. Appl. Phys.* **2000**, *87*, 484−492.
(4) van Dover, R. B.; Schneemeyer, L. F.; Fleming, R. M.; Huggins, H. A. *Biotechnol. Bioeng.* **1999**, *61*, 217−225.
(5) van Dover, R. B.; Schneemeyer, L. F.; Fleming, R. M. *Nature* **1998**, *392*, 162−164.
(6) van Dover, R. B.; Schneemeyer, L. F. *IEEE Electron Device Lett.* **1998**, *19*, 329−331.
(7) Schneemeyer, L. F.; van Dover, R. B.; Fleming, R. M. *Appl. Phys. Lett.* **1999**, *75*, 1967−1969.
(8) Aiyer, H. N.; Nishioka, D.; Maruyama, R.; Shinno, H.; Matsuki, N.; Miyazaki, K.; Fujioka, H.; Koinuma, H. *Jpn. J. Appl. Phys., Part 2* **2001**, *40*, L81−L83.
(9) Wang, Q.; Yue, G.; Li, J.; Han, D. *Solid State Commun.* **1999**, *113*, 175−178.
(10) Gilmer, D. C.; Colombo, D. G.; Taylor, C. J.; Roberts, J.; Haugstad, G.; Campbell, S. A.; Kim, H.-S.; Wilk, G. D.; Gribelyuk, M. A.; Gladfelter, W. L. *Chem. Vap. Deposition* **1998**, *4*, 9−11.
(11) Colombo, D. G.; Gilmer, D. C.; Young, J. V. G.; Campbell, S. A.; Gladfelter, W. L. *Chem. Vap. Deposition* **1998**, *4*, 220−222.
(12) Smith, R. C.; Hoilien, N.; Taylor, C. J.; Ma, T.; Campbell, S. A.; Roberts, J.; Copel, M.; Buchanan, D. A.; Gribelyuk, M.; Gladfelter, W. L. *J. Electrochem. Soc.* **2000**, *147*, 3472−3476.
(13) Smith, R. C.; Ma, T.; Hoilien, N.; Tsung, L. Y.; Bevan, M. J.; Colombo, L.; Roberts, J.; Campbell, S. A.; Gladfelter, W. L. *Adv. Mater. Opt. Electron.* **2000**, *10*, 105−114.

10.1021/cm020900+ CCC: $25.00
Published on Web 12/06/2002

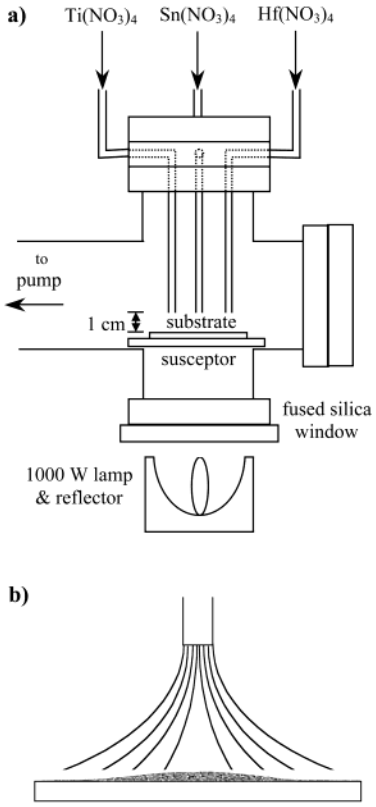

Figure 1. (a) Schematic diagram of the modified low-pressure CVD reactor showing the precursor inlet arrangement used to obtain a continuous compositional spread. (b) Schematic of the flow characteristics of an axisymmetric CVD reactor.

the chemical vapor deposition of a compositional spread (CS) of HfO_2, SnO_2, and TiO_2 from their anhydrous metal nitrate precursors using a modified low-pressure CVD reactor. A preliminary communication of this work focused on correlating the compositional spread with the dielectric properties of films deposited at 400 °C.[15] This paper includes important details on the characterization of these films and outlines the discovery of a unique crystalline phase that forms at a substrate temperature of 450 °C.

Experimental Section

CVD Precursors. Anhydrous titanium nitrate, $Ti(NO_3)_4$ [TN], was donated by Aldrich and was used as received. The anhydrous nitrates of hafnium and tin were synthesized via the reaction of the metal chloride and N_2O_5 using a modification of literature procedures.[16,17] $Hf(NO_3)_4$ [HN] and $Sn(NO_3)_4$ [SnN] were purified by sublimation. All precursors were stored and vessels were loaded under a dry N_2 atmosphere inside a glovebox. *Caution: Anhydrous metal nitrates are strong oxidants and care should be taken to avoid contact with organic compounds.*

Deposition Conditions. The cold-wall, low-pressure CVD reactor has been described in detail previously.[12] The precursor delivery apparatus was modified such that the precursor outlets were extended directly over the substrate surface at a height of 1 cm (Figure 1a). The close proximity of the outlets to the substrate significantly increased the deposition rate for each oxide.

Substrates were Si(100) wafers cut into pieces of approximately 24 × 24 mm. The wafer pieces were degreased using methylene chloride, blown dry, and then placed into a solution consisting of 7 parts concentrated H_2SO_4 and 3 parts 30% H_2O_2. Immediately prior to deposition a wafer was removed from the solution, rinsed thoroughly with deionized water, dipped into a 10% hydrofluoric acid solution for 15 s to remove the native oxide, and blown dry. The wafer piece was then placed immediately onto the susceptor and centered below the precursor outlets. The deposition chamber was evacuated for a minimum of 20 min prior to deposition.

After the evacuation procedure, the N_2 carrier gas flow into the chamber was started, bypassing the precursor vessels. The TN and HN precursor vessels were heated using Variac-controlled heating tape and the SnN vessel was cooled using an ice water bath. All delivery lines were heated to approximately 75 °C. The susceptor was heated using a 1000 W halogen lamp. In this study, compositional spread samples were deposited at 400 °C and 450 °C. Once the precursor vessels and susceptor reached their desired temperatures the carrier gas flows were simultaneously directed through the precursor vessels. The total reactor pressure was 0.4 Torr during a deposition.

For the 400 °C depositions, approximately equivalent deposition rates were achieved using nitrogen carrier gas flow rates of 15, 10, and 20 sccm through the $Ti(NO_3)_4$, $Sn(NO_3)_4$, and $Hf(NO_3)_4$ vessels, respectively. The TN and HN vessels were heated to 40 and 60 °C and the SnN vessel was cooled to 0 °C in an ice bath. When a 450 °C deposition temperature was used, growth rates were approximately equivalent for carrier gas flow rates of 10, 25, and 5 sccm and vessel temperatures of 15, 70, and 0 °C for the TN, HN, and SnN vessels. Under these conditions reproducible deposition rates of 60−100 nm/min, measured at the center points under each precursor outlet, were achieved.

Two films of $Ti_xSn_yHf_zO_2$ with a single composition were deposited at 400 °C using the chamber without the modified precursors outlets in place. For these films the precursor vessels were maintained at 25, 0, and 70 °C for the TN, SnN, and HN vessels, respectively. For the first sample a composition of $Ti_{0.78}Sn_{0.13}Hf_{0.09}O_2$ was obtained using N_2 flow rates of 15, 5, and 25 sccm through the TN, SnN, and HN vessels. Carrier gas rates of 10, 5, and 50 sccm resulted in the composition $Ti_{0.51}Sn_{0.22}Hf_{0.27}O_2$ for the second film. Under these conditions, the observed deposition rate was 10 nm/min.

For the 450 °C deposition temperature, a sample with composition $Hf_{0.69}Sn_{0.31}O_2$ was grown using 50 and 10 sccm N_2 flow rates and 65 and 0 °C vessel temperatures for HN and SnN, respectively. The observed deposition rate was 6.5 nm/min.

Thin Film Characterization. The lower left corner of all thin films was designated as the origin point, thus the sample area corresponded to the positive (x, y) quadrant of a Cartesian coordinate system. The location of a given analysis point could then be denoted by the x and y coordinates.

Rutherford backscattering spectrometry was performed using a spectrometer purchased from NEC and equipped with a MAS 1700 end station. The energy of the He^+ beam was 2.0 MeV and the beam current was 15 nA. The diameter of the beam in the RBS experiment was 1−2 mm. Using a video camera within the instrument sample chamber and a computer controlled goniometer, the He^+ beam could be focused at specific locations on the sample surface and the locations could be saved in a sample queue. For the samples containing a compositional spread, up to 100 individual spectra, arranged in a 10 × 10 array covering the majority of the sample area, were acquired. The RBS spectrum at each location was modeled by a composition corresponding to $Ti_xSn_yHf_zO_2$ ($x + y + z = 1$), where x, y, and z were calculated from the atomic percentage of each metal obtained in the experiment. The total charge collected for each spot in the compositional spread was 5 μC. For samples containing a single composition 10 μC was collected at 5 spots that were randomly arranged across the

(14) Taylor, C. J.; Gilmer, D. C.; Colombo, D. G.; Wilk, G. D.; Campbell, S. A.; Roberts, J.; Gladfelter, W. L. *J. Am. Chem. Soc.* **1999**, *121*, 5220−5229.
(15) Smith, R. C.; Hoilien, N.; Roberts, J.; Campbell, S. A.; Gladfelter, W. L. *Chem. Mater.* **2002**, *14*, 474−476.
(16) Schmeisser, M. *Angew. Chem.* **1955**, *67*, 493−501.
(17) Field, B. O.; Hardy, C. J. *Proc. Chem. Soc.* **1962**, 76−77.

Table 1. Relative Sizes of the Analytical Probes Used to Characterize These Films[a]

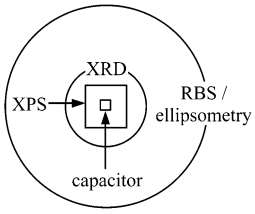

analysis technique employed	measure of interest	probe dimension (mm)	shape of area probed	range of slope (unit/mm)	median slope (unit/mm)	Δ across 0.1 mm at median
RBS	% Ti	2.0	circle	0.0059−7.3%	0.67%	0.067%
	% Sn			0.071−6.3%	1.6%	0.16%
	% Hf			0.021−6.3%	2.5%	0.25%
XPS	% Ti	0.40	square	0.030−7.7%	0.57%	0.057%
	% Sn			0.0059−7.8%	1.4%	0.14%
	% Hf			0.041−7.6%	2.6%	0.26%
ellipsometry	thickness	1.0−2.5[b]	ellipse	0.017−3.8 nm	0.26 nm	0.026 nm
XRD	crystallinity	0.8−1.2[b]	ellipse	n/a	n/a	n/a
capacitor	electrical	0.10	square	n/a	n/a	n/a

[a] The variation of the results for each method over the analysis area and across a distance equivalent to one capacitor (100 mm) is also noted. [b] The range describes the dimensions of the two axes formed by reflecting the circular beam at an angle other than 90°.

wafer surface. The spectra were indistinguishable, confirming that within the limits of the instrument the composition and thickness were identical across each sample.

X-ray photoelectron spectroscopy was performed at Evans PHI using a Physical Electronics Quantum 2000 Scanning XPS using monochromatic Al Kα radiation. The XPS spectra for the Ti 2p, Sn 3d, and Hf 4f transitions were collected at a 45 ° takeoff angle on 625 individual (arranged in a 25 × 25 array) 400 × 400 μm squares. To avoid altering the metal ratios, the spectra were obtained without sputter cleaning the sample surface.

Film crystallinity was evaluated using a Bruker AXS X-ray microdiffractometer fitted with a Hi-Star 2-D area detector. A 2.2-kW sealed Cu X-ray source was used to generate the X-rays, which were passed through a 0.8-mm beam collimator. Using a video microscope and laser, the collimated X-ray beam could be precisely focused onto individual locations on the films, which were mounted onto the 1/4 Eulerian cradle sample holder. The XRD spectra were collected for 10 min using general area detector diffraction software (GADDS). Samples were rotated during data collection to ensure sampling of all film orientations.

Ellipsometry at 70° incident radiation ($\lambda = 632.8$ nm) was used to measure the film thickness, and these results agreed well with thickness evaluations obtained by RBS. The refractive index ranged from 1.95 to 2.3. Samples for X-ray diffraction and RBS analysis were typically 80−250 nm thick. Samples grown at 400 °C ranging in thickness from 9.5 to 50 nm (this range refers to that found on a single wafer) were used for XPS measurements and for preparation of capacitor arrays. For the 450 °C CS, capacitors were patterned on a sample ranging from 10 to 25 nm. Capacitors were also fabricated on single composition samples with thickness ∼6 nm.

Electrical Characterization. Using standard lithography methods, arrays of 100 × 100 μm capacitors were prepared. Platinum was used as the top electrode and was deposited using a dc sputtering process. Capacitance−voltage (C−V) properties were examined using an HP 4294A impedance analyzer, and current−voltage (I−V) measurements were acquired on an HP 4156A parameter analyzer. Counting from the measurable device nearest to the origin (lower left corner of capacitor array), the C−V and I−V spectra were collected every 15 capacitors from −2 to 2 V. The location relative to the origin was then determined by multiplying the (*x*, *y*) designation for each capacitor by 120 μm, which corresponded to the distance between the centers of adjacent devices. The value of capacitance was extracted for a gate bias of −1.5 V for each device. This value for the gate bias was chosen because it was well within the accumulation region for all devices. The effective dielectric constant, κ_{eff}, was calculated using the thickness obtained from ellipsometry and eq 1, then mapped.

$$C = \frac{\kappa \epsilon_0 A}{t} \tag{1}$$

Results

Compositional Spreads Deposited at 400 °C. *Analytical Methods.* Table 1 summarizes the relative beam sizes of the analytical methods used in this study. For each technique, the variation over 100 μm (the size of one capacitor) was calculated using the largest difference between adjacent points and thus represents the maximum change in composition or thickness expected across a capacitor. For XPS and RBS the concentrations of Ti, Hf, and Sn in the compositional spreads varied by a maximum of ∼0.8% across a 100-μm capacitor. The thickness, as measured by ellipsometry, varied by a maximum of ∼0.4 nm over the same distance.

Composition Mapping. Figure 2 (parts a−c) shows the elemental concentration (in percent) of Ti, Sn, and Hf as a function of position within a 9−50-nm-thick CS sample grown at 400 °C. The metal concentrations were derived from the intensities of the Ti 2p, Sn 3d, and Hf 4f regions in the 25 × 25 array of X-ray photoelectron spectra after applying intrinsic sensitivity factors. Approximately 25% of the total sample area was analyzed by this procedure, and the concentrations of the intervening areas were interpolated.

A 6 × 6 array of Rutherford backscattering spectra was obtained for a 120−250-nm-thick CS film deposited under conditions identical to those of the thin sample analyzed by XPS. The RBS spectra were modeled well by compositions corresponding to $Ti_xSn_yHf_zO_2$, where the sum of *x*, *y*, and *z* was equal to one. Comparison by a *t* test of the metal concentrations for identical locations within the two compositional maps established that the two analysis methods agreed. Rutherford backscattering provides a measure of the composition throughout the entire film thickness. Thus, we can conclude (1) that the surface compositions measured by XPS were representative of those found throughout the film and (2)

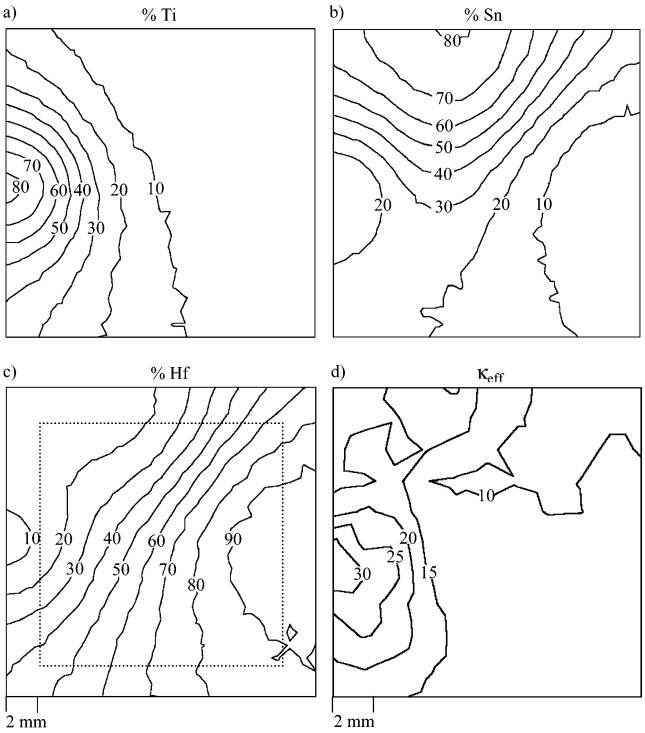

Figure 2. Compositional maps for 400 °C CS films derived from a 25 × 25 array of XPS measurements, percentages are based on the metal content only. The position scale is identical for the (a) Ti, (b) Sn, and (c) Hf maps. (d) Map of the effective dielectric constant obtained from the region indicated by the box within 2c.

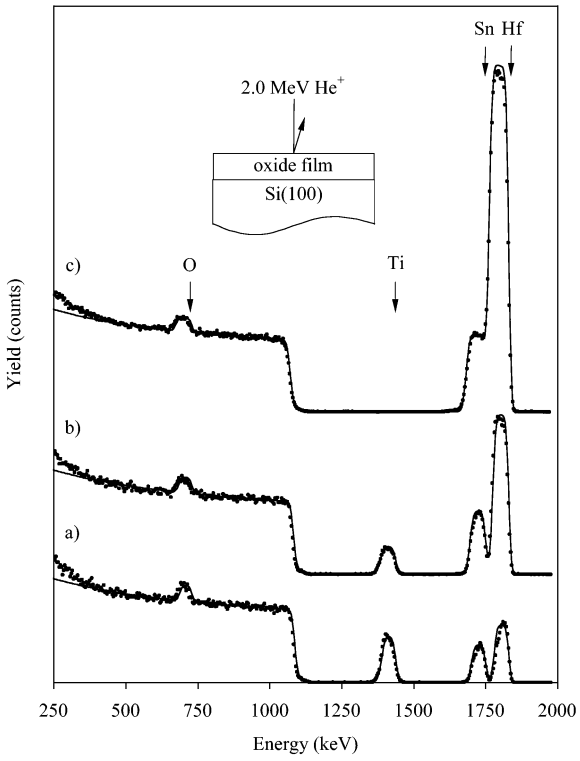

Figure 3. Plot showing the Rutherford backscattering spectra for samples having a single composition. The spectra were modeled by compositions corresponding to a mixture of titanium, tin, and hafnium oxides. Films shown in (a) 80 nm of $Ti_{0.78}Sn_{0.13}Hf_{0.09}O_2$ and (b) 85 nm of $Ti_{0.51}Sn_{0.22}Hf_{0.27}O_2$ were deposited at 400 °C, whereas (c) 100 nm of $Hf_{0.69}Sn_{0.31}O_2$ was grown at 450 °C.

that the compositional spread was independent of the film thickness.

Film Crystallinity. X-ray microdiffraction of the 400 °C CS film showed that, with the exception of the areas immediately beneath the $Ti(NO_3)_4$ and $Hf(NO_3)_4$ precursor outlets, the as-deposited films were amorphous. In the region of highest TiO_2 concentration, diffraction peaks were observed at $2\theta = 25.2°$ and 47.9° due to the 101 and 200 planes of the anatase phase. Broad reflections at $2\theta = 28.3°$, 31.5°, 35.2°, and 50.4° were present in the deposition zone below the HN injector and could be attributed to the $\bar{1}11$, 111, 002, and 022 planes of monoclinic HfO_2.

Electrical Properties. Figure 2d shows the value of κ_{eff} as a function of position within the 400 °C CS sample. The effective dielectric constant increased as the relative amount of Ti in the film increased. The composition that gave the highest κ_{eff} value (~31) was $Ti_{0.76}Sn_{0.14}Hf_{0.10}O_2$. An SiO_x interfacial layer approximately 2 nm thick has been observed in studies of metal oxides on silicon.[12,13,18−22] The effect of the interfacial layer on the value of κ_{eff} was not quantified, but the presence of this layer will reduce the capacitance for the stack.

Leakage current densities across the CS film ranged from 10^{-5} to 10^{-2} A/cm^2. Over the range of thicknesses more than one charge transport mechanism can be operative, therefore the dependence of the leakage current on the film thickness cannot be expressed by a single relationship. An empirical comparison of the leakage currents across regions of similar thickness, however, leads to a rough correlation between increasing leakage current and increasing tin concentration in the dielectric layer. The lowest values of leakage current generally were found in regions of high Hf concentrations (>70%). This is consistent with the higher band gap of HfO_2 (5.8 eV) compared to those of TiO_2 and SnO_2.

To examine more closely those compositions predicted to have high κ values or low leakage currents, films with a uniform composition were grown. Figure 3(a and b) shows the RBS spectra for these films. The spectra were modeled by layers corresponding to 80 nm of $Ti_{0.78}Sn_{0.13}Hf_{0.09}O_2$ and 85 nm of $Ti_{0.51}Sn_{0.22}Hf_{0.27}O_2$. For each sample, RBS was performed at five different locations on the wafer. The spectra were identical, confirming that composition and thickness were consistent across the entire sample surface. Thickness measurements by ellipsometry showed variation of <3% from the center to edge of the samples.

At −1.5 V gate bias, the capacitance was 2.5 μF/cm^2 and 1.6 μF/cm^2 for 6-nm-thick films of $Ti_{0.78}Sn_{0.13}Hf_{0.09}O_2$ and $Ti_{0.51}Sn_{0.22}Hf_{0.27}O_2$, respectively. The leakage current at −1.0 V was 10^{-1} to 10^{-2} A/cm^2 for both samples. The capacitance observed for the samples

(18) Yoon, Y. S.; Kang, W. N.; Yom, S. S.; Kim, T. W.; Jung, M.; Park, T. H.; Seo, K. Y.; Lee, J. Y. *Thin Solid Films* **1994**, *238*, 12−14.
(19) Son, K.-A.; Mao, A. Y.; Kim, B. Y.; Liu, F.; Pylant, E. D.; Hess, D. A.; White, J. M.; Kwong, D. L.; Roberts, D. A.; Vrtis, R. N. *J. Vac. Sci. Technol. A* **1998**, *16*, 1670−1675.
(20) Rausch, N.; Burte, E. P. *Microelectron. Eng.* **1992**, *19*, 725−728.
(21) Klein, T. M.; Niu, D.; Epling, W. S.; Li, W.; Maher, D. M.; Hobbs, C. C.; Hedge, R. I.; Baumvol, I. J. R.; Parsons, G. N. *Appl. Phys. Lett.* **1999**, *75*, 4001−4003.
(22) Alers, G. B.; Werder, D. J.; Chabal, Y.; Lu, H. C.; Gusev, E. P.; Garfunkel, E.; Gustafsson, T.; Urdahl, R. S. *Appl. Phys. Lett.* **1998**, *73*, 1517−1519.

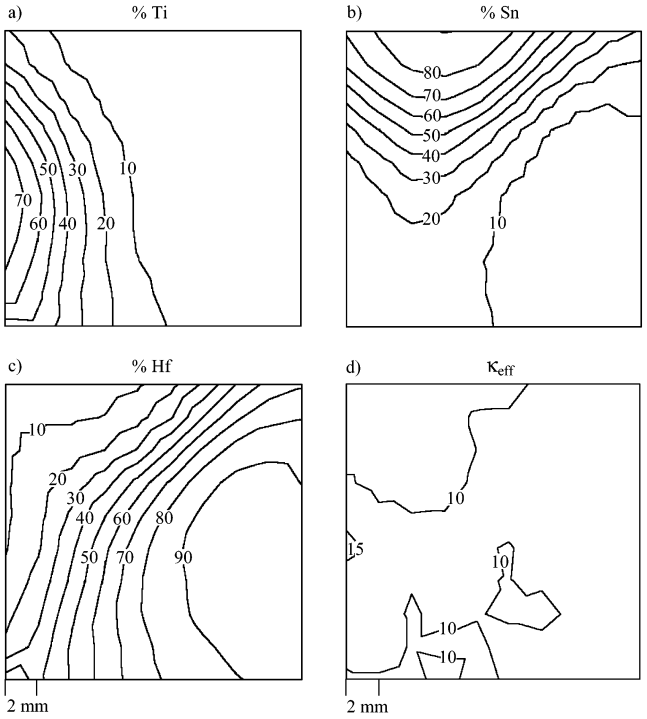

Figure 4. Compositional maps for 450 °C CS films derived from a 10 × 10 array of RBS measurements, percentages are based on the concentration of only (a) Ti, (b) Sn, and (c) Hf maps. (d) Map of the effective dielectric constant. The length scale is the same for the four maps.

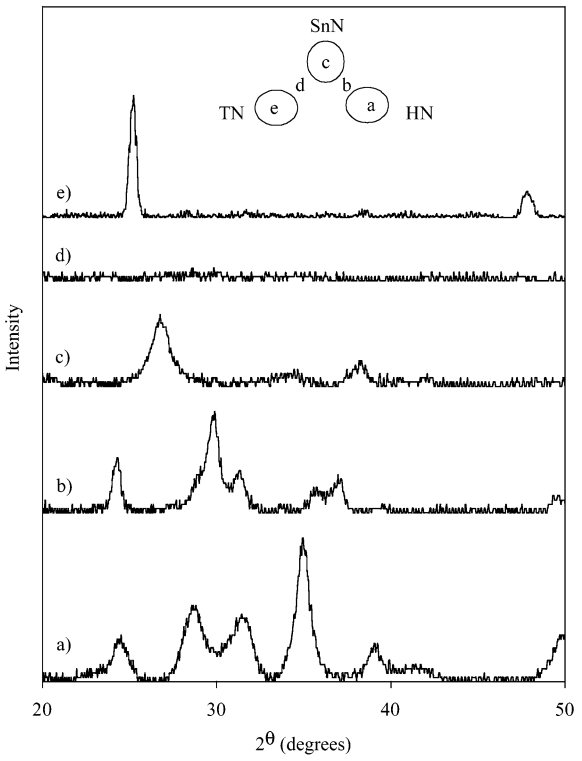

Figure 5. X-ray diffraction spectra for several locations of CS films deposited at 450 °C. Analysis positions are indicated by the inset diagram and the ellipses outline the location of the precursor outlets.

corresponded to κ_{eff} values equal to 17 and 11. For the $Ti_{0.51}Sn_{0.22}Hf_{0.27}O_2$ film the effective dielectric constant compares well to the value observed in the array of capacitors from the continuous spread of Ti, Sn, and Hf oxides. The κ_{eff} for the $Ti_{0.78}Sn_{0.13}Hf_{0.09}O_2$ film is lower than that observed in the compositional spread, but no attempt was made to account for the contribution of the interfacial SiO_x layer present at the surface. The film thickness for the single composition sample was less than that used in the compositional spread (48 nm), thus the contribution of the low κ interfacial layer may be increased, leading to the reduced dielectric constant.

Compositional Spread Deposited at 450 °C. *Composition and Electrical Mapping.* The concentrations of Ti, Sn, and Hf for the CS sample grown at 450 °C are illustrated in Figure 4a−c. The compositions were determined from a 10 × 10 array of RBS spectra, each modeled by a composition corresponding to $Ti_xSn_yHf_zO_2$ (where $x + y + z = 1$). The map of κ_{eff} with respect to position is shown in Figure 4d. Similar to the 400 °C sample, the dielectric constant increased with increasing titanium concentration, though in general the values for κ_{eff} are lower than those for the 400 °C sample. It is likely that the lower values for κ_{eff} result from decreased Ti concentration throughout the film. The SiO_x interfacial layer may also have a larger influence on the observed dielectric constant. The highest value for κ_{eff} (∼17) was observed for a composition of $Ti_{0.71}Sn_{0.20}Hf_{0.09}O_2$.

Film Crystallinity. The X-ray microdiffraction results obtained for the 450 °C CS film are shown in Figure 5. The regions of the sample directly below the TN, SnN, and HN injectors yielded peaks corresponding to the thermodynamically stable forms of the corresponding oxides. Peaks at 2θ = 24.5, 28.6, 31.7, 35.1, 39.2, and 49.9° were observed in the region under the HN injector (Figure 5a) and were attributable to the 011, $\bar{1}11$, 111, 002, 021, and 022 reflections of monoclinic HfO_2. Beneath the SnN injector (Figure 5c) reflections were observed at 2θ = 26.7° and 38.6°, corresponding to the 110 and 111 planes for cassiterite SnO_2. Under the TN injector the anatase phase was observed as indicated by reflections at 2θ = 25.2° and 47.9° due to the 101 and 200 planes (Figure 5e). Figure 5b shows that for a spot located midway between the TN and SnN injectors the film was amorphous to X-rays. Between the HN and SnN injectors (Figure 5d) diffraction observed at 2θ = 24.4, 29.9, 31.4, 35.8, 37.2, and 49.6° could not be correlated to planes in either SnO_2 or monoclinic HfO_2. The composition for this location, determined from the RBS map, was $Ti_{0.03}Sn_{0.25}Hf_{0.72}O_2$. Recently, Sleight and co-workers reported the synthesis and characterization of single-crystal samples with composition $Hf_{0.75}Sn_{0.25}O_2$ that exhibited the α-PbO_2 structure.[23] Comparison of the reflections observed in the CS film to a diffraction pattern calculated from the single-crystal data suggests the α-PbO_2 structure is present in the 450 °C spread. The α-PbO_2 structure does not exist for HfO_2, TiO_2, ZrO_2, or SnO_2 under normal conditions but does exist for some solid solutions of these oxides, including ZrO_2−TiO_2, HfO_2−TiO_2, ZrO_2−SnO_2, and ZrO_2−TiO_2−SnO_2.[24−28]

(23) Mackay, R.; Sleight, A. W.; Subramanian, M. A. *J. Solid State Chem.* **1996**, *121*, 437−442.
(24) Wolfram, G.; Gobel, H. E. *Mater. Res. Bull.* **1981**, *16*, 1455−1464.
(25) Wakino, K.; Minai, K.; Tamura, H. *J. Am. Ceram. Soc.* **1984**, *67*, 278−281.
(26) McHale, A. E.; Roth, R. S. *J. Am. Ceram. Soc.* **1986**, *69*, 827−832.

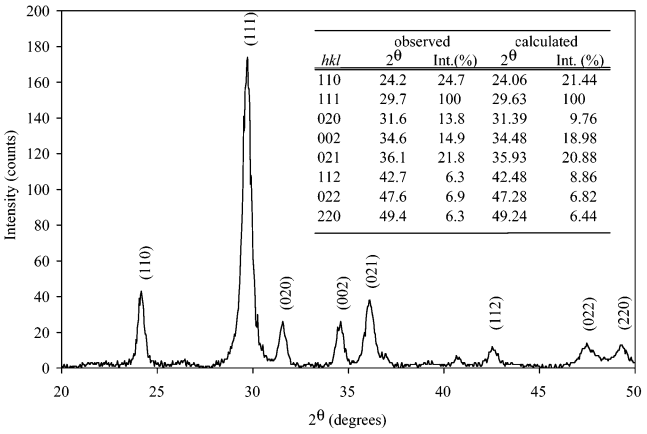

Figure 6. X-ray diffraction spectrum for a film with composition $Hf_{0.69}Sn_{0.31}O_2$ deposited at 450 °C. The inset table compares the observed values for 2θ and peak intensity to those calculated for $Hf_{0.75}Sn_{0.25}O_2$ with orthorhombic α-PbO_2 phase.

Figure 7. Scanning electron micrograph image of the surface of a 100-nm-thick $Hf_{0.69}Sn_{0.31}O_2$ film deposited at 450 °C.

To confirm the presence of the orthorhombic α-PbO_2 phase, a single composition HfO_2-SnO_2 sample was deposited at 450 °C. Rutherford backscattering, shown in Figure 3c, established the composition to be $Hf_{0.69}Sn_{0.31}O_2$. The X-ray microdiffraction pattern for $Hf_{0.69}Sn_{0.31}O_2$ (Figure 6) exhibited peaks at $2\theta = 24.1$, 29.7, 31.6, 34.6, 36.1, 42.5, 47.5, and 49.4° that corresponded to the 110, 111, 020, 002, 021, 112, 022, and 220 reflections, respectively. Figure 7 shows a plan-view SEM image of a 100-nm-thick film of $Hf_{0.69}Sn_{0.31}O_2$ that reveals a randomly oriented polycrystalline film with an elongated grain structure. The value of κ_{eff} for a location with $Ti_{0.02}Sn_{0.22}Hf_{0.76}O_2$ in the 450 °C compositional spread sample was 14, which is in close agreement with the value ($\kappa = 13$) measured by Sleight and co-workers for the single crystals.[23]

Table 2. Thickness Comparison of Locations Within Four Independently Grown Samples (TiO_2, SnO_2, HfO_2, and $Ti_xSn_yHf_zO_2$)[a,b]

location[a]	SnO_2 only (nm)	TiO_2 only (nm)	HfO_2 only (nm)	sum (nm)	CS film (nm)
1	124	42	14	180	152
2	278	15	35	328	271
3	105	5	88	198	155
4	83	219	15	317	282
5	185	38	58	281	244
6	65	7	116	188	145
7	26	300	14	340	352
8	54	40	65	159	121
9	17	5	236	258	257

[a] Films were deposited at 400 °C using TN (40 °C, 15 sccm), SnN (0 °C, 10 sccm), and HN (60 °C, 20 sccm). For the single component depositions, pure carrier gas was allowed to flow through the other outlets at the same velocity used during the combined deposition. In the experiments, the distance between columns was 8 mm and the distance between rows was 4 mm. [b] Legend:

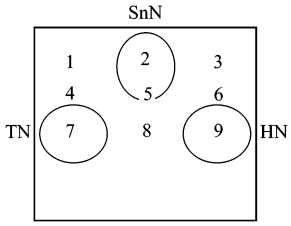

Discussion

The primary goal of this work was to balance the reactor fluid dynamics and precursor deposition kinetics to create a continuous compositional spread of TiO_2, SnO_2, and HfO_2 on a single wafer. Ideally, one would like to use this wafer to measure physical properties for any value of x, y, and z for $Ti_xSn_yHf_zO_2$ where x, y, and z range from 0 to 1 and where $x + y + z = 1$. In this study, the dielectric constant was correlated to the film composition. Figure 1b shows a rough schematic of the gas flow pattern in an axisymmetric CVD reactor. The precursor molecules react at the substrate surface after diffusing across the flow streamlines. Because this depletes the precursor concentration, its flux, and ultimately the film thickness, decreases as the radial distance from the center point increases. Under typical deposition conditions experimentation established that the film thickness dropped to approximately 25% of its maximum value at a radius of 1 cm. By spacing the precursor outlets at this distance, varying amounts of each metal oxide would be deposited at each point on the substrate.

Table 2 compares the film thickness for individual depositions to those obtained for the co-deposition under the same conditions. To minimize the impact on the fluid dynamics in the single deposition of TiO_2, pure carrier gas was directed through the SnO_2 and HfO_2 outlets at the velocities used in the co-depositions. The analogous setup was used for the single depositions of SnO_2 and HfO_2. For each deposition the thickness was measured at an identical set of nine locations on the substrate. Over the entire substrate, the sum of the individual component thicknesses matches the thick-

(27) Kudesia, R.; McHale, A. E.; Condrate, R. A., Sr.; Snyder, R. L. *J. Mater. Sci.* **1993**, *28*, 5569−5575.
(28) Kudesia, R.; Snyder, R. L.; Condrate, R. A., Sr.; McHale, A. E. *J. Phys. Chem. Solids* **1993**, *54*, 671−684.

ness measured for the combined deposition within 20%. This suggests that any one of the metal oxides neither poisons nor accelerates the deposition of another; a factor at least in part due to the similar deposition chemistry resulting from the common nitrate ligand among the three precursors.

Film Microstructure. Several possible microstructures for the mixed oxides could arise within the CS films. At one extreme, the resultant mixed oxide film could be completely homogeneous. In this case the relative number of M−O−M, M−O−M′, M−O−M″, and M′−O−M″ bonds would reflect a statistical distribution of the oxide components. At the other extreme, complete phase segregation possibly accompanied by crystallization of the component oxides could occur. A third case could involve the formation of regions of crystalline MO_2 within an amorphous matrix of mixed oxides. Finally, two or more of the component oxides may react to form a new material that phase separates. An example of this last case is the formation of the orthorhombic $Hf_{0.75}Sn_{0.25}O_2$ phase within the 450 °C CS sample. Elsewhere on this sample (see Figure 5), regions that contained high concentrations of individual components formed the corresponding stable, crystalline phase. The only exception to this was the area between the SnO_2 and TiO_2 centers, which remained amorphous. Presumably the minor components exist as an amorphous matrix in the grain boundary regions, but more detailed microscopy would be needed to verify this. For the CS films deposited at 400 °C all regions were amorphous to X-rays except those immediately beneath the TiO_2 and HfO_2 precursor outlets.

Electrical Properties. The values of κ_{eff} observed in the CVD-grown compositional spread were reasonably predicted by the linear combination of the component dielectric constants weighted by their relative concentrations. Using the above assumption the best-fit values of κ_{eff} were 35, 17, and 10 for TiO_2, HfO_2, and SnO_2, respectively. These results are comparable to those reported in the literature for amorphous or polycrystalline films.[10,29−32] The thickness of the interfacial SiO_x layer was not independently measured and no attempt was made to extract the contribution of the layer from the electrical results. In our previous studies of TiO_2 deposited from TN the interfacial layer thickness was ∼2 nm, whereas for HN-deposited HfO_2 the interfacial layer thickness was ∼1.5 nm.[10,13] The presence of this SiO_2-rich interfacial layer effectively reduces the value of κ_{eff} observed for the total film. The above calculation also neglected the impact of changes in the molar volume of the mixed oxides.[33]

Two issues complicate direct comparison of the electrical properties obtained in this study to those observed in CS films deposited by sputtering. First, the substrate temperatures in the off-axis reactive sputtering deposition were significantly lower (200−300 °C) than those used in this study. This may cause changes in the film microstructure that impact the dielectric behavior. Although anhydrous metal nitrates can be used to deposit films at low temperatures, the deposition time is significantly increased. Second, the figure of merit used by Schneemeyer et al. was based on the maximum amount of charge that could be stored on a capacitor (= capacitance × breakdown voltage). The highest figure of merit observed in their study corresponded to $Ti_{0.75}Sn_{0.05}Hf_{0.20}O_2$.[7] The highest value of κ_{eff} observed in our study corresponded to the compositions $Ti_{0.76}Sn_{0.14}Hf_{0.10}O_2$ and $Ti_{0.80}Sn_{0.11}Hf_{0.09}O_2$ for the 400 and 450 °C films, respectively. Both methods suggest that a TiO_2−rich film will produce the highest value for κ.

Summary

A modified CVD reactor was used to deposit compositional spreads of TiO_2, SnO_2, and HfO_2 using the respective anhydrous metal nitrates as single-source precursors. From an array of capacitors, electrical measurements established that the dielectric constant was a maximum for films having the highest TiO_2 content. Additionally, X-ray microdiffraction measurements revealed the formation of the orthorhombic α-PbO_2 structure in films with composition close to $Hf_{0.75}Sn_{0.25}O_2$ deposited at 450 °C. This experimental methodology will enable the exploration of dielectric properties of multicomponent metal oxide films deposited by CVD, as well as the connection between film composition and other important physical properties.

Acknowledgment. This research was supported by funds from the National Science Foundation [CHE-0076141] and the Semiconductor Research Corporation. We acknowledge Dr. Victor G. Young for simulation of the XRD powder patterns for $Hf_{0.75}Sn_{0.25}O_2$.

CM020900+

(29) Campbell, S. A.; Gilmer, D. C.; Wang, X.; Hsieh, M.; Kim, H.-S.; Gladfelter, W. L.; Yan, J. *IEEE Trans. Electron. Dev.* **1997**, *44*, 104−109.

(30) Van Daal, H. J. *J. Appl. Phys.* **1968**, *39*, 4467−4469.

(31) Ma, T.; Campbell, S. A.; Smith, R.; Hoilien, N.; He, B.; Gladfelter, W. L.; Hobbs, C.; Buchanan, D.; Taylor, C.; Gribelyuk, M.; Tiner, M.; Copel, M.; Lee, J. J. *IEEE Trans. Electron. Dev.* **2001**, *48*, 2348−2356.

(32) Huber, F. *IEEE Trans. Parts, Hybrids, Packag.* **1971**, *7*, 141−147.

(33) Devine, R. A. B.; Revesz, A. G. *J. Appl. Phys.* **2001**, *90*, 389−393.